



Contents lists available at ScienceDirect

Nuclear Instruments and Methods in Physics Research B

journal homepage: [www.elsevier.com/locate/nimb](http://www.elsevier.com/locate/nimb)

## Target nanomaterials at CERN-ISOLDE: synthesis and release data

J.P. Ramos<sup>a,b,\*</sup>, A. Gottberg<sup>a,1</sup>, R.S. Augusto<sup>a,c</sup>, T.M. Mendonca<sup>a</sup>, K. Riisager<sup>d</sup>, C. Seiffert<sup>a,e</sup>, P. Bowen<sup>b</sup>, A.M.R. Senos<sup>f</sup>, T. Stora<sup>a,\*</sup>

<sup>a</sup> ISOLDE, CERN, CH-1211 Genève 23, Switzerland

<sup>b</sup> Laboratory of Powder Technology, EPFL, CH-1015, Switzerland

<sup>c</sup> Department of Physics, Ludwig-Maximilians-University, Munich, Germany

<sup>d</sup> Department of Physics and Astronomy, University of Aarhus, DK-8000 Aarhus, Denmark

<sup>e</sup> Technische Universität Darmstadt, Schlossgartenstraße 9, 64289 Darmstadt, Germany

<sup>f</sup> Department of Materials and Ceramics Engineering, University of Aveiro, CICECO, 3810-193 Aveiro, Portugal

### ARTICLE INFO

#### Article history:

Received 31 August 2015

Received in revised form 17 December 2015

Accepted 1 March 2016

Available online xxxx

#### Keywords:

Nanomaterials

CERN-ISOLDE

Spallation recoil

Release efficiency

Radioactive ion beams

### ABSTRACT

Five different nanostructured target materials were tested and operated at ISOLDE in the year of 2014, three of them being carbon-based nanocomposites. In most cases such target materials have higher radioisotope intensities than standard targets and with apparently longer release characteristics. Here, an isotope release profile from a standard calcium oxide (CaO) powder target is compared to the nanostructured one. For all target materials, the synthesis is the key process since it determines the material characteristics and maximum operation temperature which, in turn, defines the final isotope yields (especially for exotic isotopes). An unexpected release of Ar isotopes from a nanometric CaO powder target, with its oven set to room temperature is described and a release mechanism is proposed: spallation recoil momentum from the  $^{nat}\text{Ca}(p,x)^{35}\text{Ar}$  reaction.

© 2016 The Authors. Published by Elsevier B.V. This is an open access article under the CC BY-NC-ND license (<http://creativecommons.org/licenses/by-nc-nd/4.0/>).

### 1. Introduction

The ISOLDE (Isotope Separator OnLine DEvice) facility at the European Organization for Nuclear Research, CERN, went through several upgrades during the long CERN-wide accelerator shutdown in 2013 to accommodate the HIE-ISOLDE (HIE as in High Energy) programme that will lead to higher reaccelerated beam energies and beam intensities. The installation of the first cryomodule with a set of superconducting high-beta cavities is one of the highlights which will provide, post-accelerated radioactive ion beams up to 4.3 MeV/u, in the coming months and 5.5 MeV/u for  $A/q = 4.5$  at the beginning of 2016. The Test Storage Ring (TSR) at CERN to be installed as part of the HIE-ISOLDE project and the ISOLDE target area extension – MEDICIS (MEDical Isotopes Collected from ISO-LDE) [1] – will create a very dynamic and unique facility in the world, opening doors for new physics and new applications [2]. The long shutdown of 2013 has also allowed much progresses from the target and ion source development team at ISOLDE, bringing

new target materials with tailored nanostructures, development of new target concepts and prototype units tested in 2014/2015.

In the field of liquid targets, while an innovative molten Pb:Bi loop target (LIEBE Liquid Eutectic Lead Bismuth Loop Target for EURISOL – European Isotope Separator OnLine) is in development, a second molten NaF:LiF salt prototype target delivered good and reproducible intensities of  $^{11}\text{CO}$  and  $^{18}\text{Ne}$  beams [2–4]. In total, 5 nanomaterial targets were tested at ISOLDE with engineered highly porous nanostructures to enhance the release rates of short lived isotopes. This includes titanium carbide (TiC), a newcomer to ISOLDE, mixed with carbon black to create a nanocomposite (Fig. 1c) very stable at high temperatures (up to 2000 °C) [5]. Two other nanocomposites based on multiwall carbon nanotubes (MWCNT) – lanthanum carbide ( $\text{LaC}_x$ ) [6] and uranium carbide ( $\text{UC}_x$ ) [7] – and a target fully made of MWCNT (Fig. 1a and b) were also successfully tested online [8,9]. A nanometric calcium oxide powder (CaO) [10], which is no longer a prototype target, was operated for the first time with its oven set to room temperature to unexpectedly deliver intense Ar beams.

If the isotope release is diffusion limited, and the isotope half-life sets the typical diffusion time which is required to prevent dominant losses during the release process, increasing the temperature ( $T$ ), accelerates the diffusion ( $D$ ) in  $[\text{m}^2 \text{s}^{-1}]$  following an Arrhenius expression:

\* Corresponding authors at: ISOLDE, CERN, CH-1211 Genève 23, Switzerland (J.P. Ramos).

E-mail addresses: [joao.pedro.ramos@cern.ch](mailto:joao.pedro.ramos@cern.ch) (J.P. Ramos), [thierry.stora@cern.ch](mailto:thierry.stora@cern.ch) (T. Stora).

<sup>1</sup> Present address: TRIUMF, 4004 Wesbrook Mall, Vancouver, BC V6T 2A3, Canada.

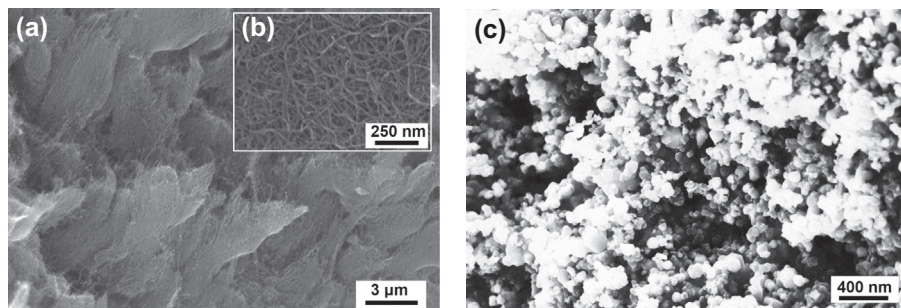


Fig. 1. Examples of nanomaterials at ISOLDE: MWCNT (a) and detail (b), titanium carbide, carbon black nanocomposite (c).

$$D = D_0 \exp\left(-\frac{Q}{RT}\right) \quad (1)$$

where  $Q$ ,  $R$  and  $D_0$  are respectively the activation energy [ $\text{J mol}^{-1}$ ], the ideal gas constant [ $\text{J K}^{-1} \text{mol}^{-1}$ ] and the diffusion pre-exponential factor [ $\text{m}^2 \text{s}^{-1}$ ]. In Isotope Separator OnLine (ISOL) facilities the solid targets are traditionally operated at as high a temperature as possible. This causes degradation of release efficiency due to an increase of the particle size and decrease of porosity by sintering, which can also be influenced by the defect creation from the proton irradiation [11].

Alternatively, to accelerate the release process, one can reduce the particle size of the target material by orders of magnitude, by engineering nanostructures. The release efficiency ( $\varepsilon_{\text{rel}}$ ), if limited by diffusion, can be approximated by the following formula (assuming spherical particles) [12]:

$$\varepsilon_{\text{rel}} = \frac{3}{\pi} \sqrt{\frac{\mu_s}{\lambda}} \quad \text{with } \mu_s = \frac{\pi^2 D}{r^2} \quad \text{and } 2\mu_s \lesssim \lambda \quad (2)$$

where  $r$  is the particle radius [m],  $\mu_s$  is the diffusion time [ $\text{s}^{-1}$ ] and  $\lambda$  is the isotope's decay constant [ $\text{s}^{-1}$ ].

Unless a suitable stabilization mechanism can be employed, nanostructures often have to be operated at lower temperatures than their traditional target materials counterparts, because of their enhanced sintering kinetics, which calls for dedicated investigations in order to define the optimum temperature [13]. To hinder sintering one can either dope the material or reduce the coordination number (number of contacts) of the particles of the target material: in both cases, introducing a second refractory material which should be homogeneously distributed. This was applied for the prototype nanocomposites operated during 2014 – TiC + Carbon Black [5],  $\text{UC}_x$  + MWCNT [7] and  $\text{LaC}_x$  + MWCNT [6] – where a carbon source is used to reduce the coordination number of the primary material and as such hinder the sintering, allowing these materials to be operated at much higher temperatures.

The nanocomposites production normally involves 4 stages: (i) wet powder milling to reduce the particle size and/or the agglomerate size of the primary material, (ii) mixing both powder materials in suspension which can be done either directly in the mill or using ultrasound and constant agitation, (iii) drying of the suspension in constant agitation to avoid segregation of the nanocomposite components and finally (iv) a final manual deagglomeration of the dry product and pressing into powder compacts of 1–2 mm thickness. The powder compacts, as the standard materials, are then introduced into a support made of graphite for carbide materials or of rhenium for the oxide materials and introduced into a tantalum oven.

The pulse-like release time-structure from the nanostructured target material displays longer characteristic fall times than from other target materials and typically exhibits higher yields, as observed in the different nanomaterials operated so far.

The nanomaterials microstructure, can also favour the cases where it is only possible to release an element as a volatile molecule, due to very high specific surface area available for reaction. This was the case for the first ISOL Boron beams released from MWCNT as  $^8\text{BF}_2$  [9].

### 1.1. Release time-structure from nanostructured – CaO powder targets

Nanometric CaO powder targets were developed in 2011, and are now a standard production material at ISOLDE. This target is produced through vacuum decarbonation of calcium carbonate at  $800^\circ\text{C}$  and is composed of porous aggregates of nanometric particles ( $\sim 40 \text{ nm}$  – Fig. 2a) with very high specific surface area, SSA ( $38 \text{ m}^2 \text{g}^{-1}$ ) [10,13,14]. Previous work using this synthesis method was not carried out in a controlled manner and did not establish a temperature limit for the decomposition. These earlier CaO materials were operated at high temperatures ( $>1050^\circ\text{C}$ ), which lead to a sintering of the material (Fig. 2b) giving variable beam intensities which decreased over time. Although the target materials in Fig. 2a and b are made of the same stoichiometric CaO, the morphology is distinct with a difference of one order of magnitude in the SSA values.

At ISOLDE the typical isotope release is pulse shaped and can be mathematically defined by a triple exponential time constant-like formula, with a rise time ( $t_r$ ) and two weighted fall times: a fast fall ( $t_f$ ) and a slow fall time ( $t_s$ ) [15]. The release curves of a nanometric and a micrometric CaO material are shown in Fig. 2c and d respectively (reproduced from [10]) were taken at the end of their respective operation time and normalized to the respective pulse height. The apparent longer release characteristics from the nanostructured CaO (see  $t_s$  and  $t_f$  on Fig. 2c and d), as also seen in other nanomaterials [16], has to be considered with the comparison of the total yield, which is in this case almost 20 times higher.

The decrease of the particle size by two to three orders of magnitude is expected to greatly reduce the diffusion times. But, the nanomaterials have a much larger pore volume and also, a more complex network of open pores with very different pore size distributions. Such a microstructure affects the effusion times, since they depend on the number of wall collisions as well as the associated sticking and flight times. However, the effect of the porosity in the release properties is not discussed in this work. These profiles indicate that the radioisotope release from nanomaterials is far from trivial and that further understanding of the physical-chemical phenomena is needed. Currently, modelling of the release is ongoing [5] considering the already existing models with 1 effusion and 1 diffusion time constants from R. Kirchner [18] or with 2 effusion constants developed by Bouquerel et al. [19,20].

### 1.2. Non-trivial release – the recoil phenomena

The release process can be very complex involving many physical phenomena which are highly dependent on the material

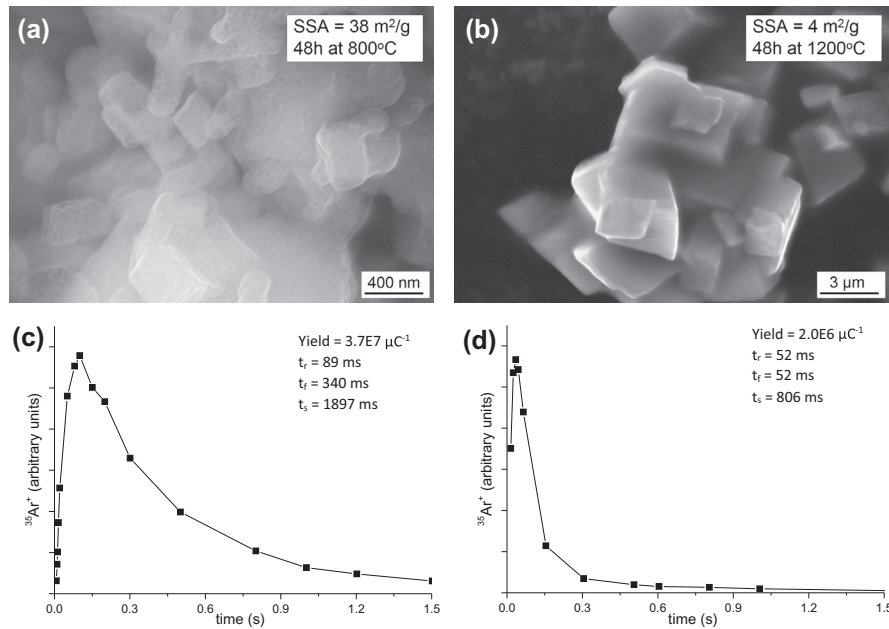


**Fig. 2.** Nanometric CaO target heat treated at the designed operation temperature –800 °C (a) and respective experimental release curve of  $^{35}\text{Ar}^+$  at the end of operation (c). Previous ISOLDE micrometric CaO target heat treated at 1200 °C (b) and respective release curve of  $^{35}\text{Ar}^+$  at the end of operation (d) – (c) and (d) reproduced from [10]. In both cases (c and d) a VADIS – Versatile Arc Discharge Ion Source was used with approx. 8% ionization efficiency for  $^{40}\text{Ar}$  [17]. Given are the time values and yields resulting from a fit using one exponential rise and two exponential fall times [15].

morphology and of its physical–chemical characteristics, as discussed above. This complexity revealed itself with the unexpected release of  $^{31}\text{Ar}$  (14.4 ms) and  $^{35}\text{Ar}$  (1.78 s), both from a nanometric CaO target operated with its oven at room temperature. The “room temperature beams” were only 2- to 3-fold less in intensity compared to the beams extracted at the standard operation temperature (~750 °C) [10]:  $^{35}\text{Ar}$  from  $2.4\text{E}7$  to  $1.0\text{E}7 \mu\text{C}^{-1}$  (Fig. 3a) and  $^{31}\text{Ar}$  from  $1.3$ – $1.9$  to  $0.6 \mu\text{C}^{-1}$ . Using Eqs. (1) and (2) and taking  $Q = 101 \text{ kJ mol}^{-1}$  and  $D_0 = 1.2\text{E}^{-13} \text{ m}^2 \text{ s}^{-1}$  from Ref. [14], for Ar diffusion in CaO and scaling for the ionization efficiency (3% on  $^{40}\text{Ar}$  for the yields in this case) the influence of the decreased temperature on the yield can be estimated to be orders of magnitude lower (diffusion assumed to be controlling the release process – see Fig. 3a).

The total energy deposition of the proton beam in the CaO nanomaterial was estimated using a Monte-Carlo particle transport simulation code FLUKA [21,22]<sup>2</sup>. The simulation’s geometry of the target; including the container (Ta oven), and the  $30 \mu\text{m}$  Re foil boat enclosing the  $0.4 \text{ g cm}^{-3}$  CaO nanomaterial, is shown in Fig. 3c. When no ohmic heating current is applied to the target oven, as is the present case, the heat contribution can only come from the  $3 \times 10^{13}$  protons per  $2.4 \mu\text{s}$  pulse (up to  $2 \mu\text{A}$ ) impact on target. Using the respective heat capacities, for every pulse, the adiabatic temperature increases around  $\sim 5 \text{ °C}$  on all the materials (4.9, 5.4 and  $4.6 \text{ °C}$  on CaO, Ta and Re, respectively). Taking into account the heat dissipation mechanisms, conduction through the CaO or thermal radiation losses, the maximum average temperature increase during irradiation from the deposited beam power of  $15 \text{ W}$  ( $1 \mu\text{A}$  of protons), would be  $\sim 280 \text{ °C}$ <sup>3</sup>. Therefore, the deposited

power from the protons would not heat up the target sufficiently in order to explain this release as a classical diffusion phenomena.

A radiation-enhanced diffusion (RED) mechanism has been reported as the responsible mechanism for higher yields by increasing the proton flux ( $\Phi$ ) on target. The yields followed a law between  $\Phi^{3/2}$  and  $\Phi^2$ , keeping the same operation temperature at TRIUMF-ISAC (TRI University Meon Facility – Isotope Separator and Accelerator in Canada’s National Laboratory for Particle and Nuclear Physics) [23,24]. This mechanism comes from the irradiation-induced creation of extra defects (Frenkel pairs – vacancies and interstitial atoms) in the crystalline structure, which significantly enhances the diffusion coefficients, especially at low temperatures. It was shown that RED is temperature-independent and more prominent at lower temperatures, since at high temperatures the defects tend to anneal out, thus cancelling the effect. At low temperatures, RED is only limited by the defect mobility which has an Arrhenius type temperature dependence (similar to Eq. (1)) [25]. In the case of this work, although the temperature is low, we don’t expect the defects in CaO to be mobile at room temperature (it has a very high melting point of  $2898 \text{ °C}$  [26]), so this effect is not likely to be responsible for the release of Ar [13].

When going to very low temperatures (room temperature) we probably observe a change in the regime that controls the release. We suspect that the  $^{35}\text{Ar}$  spallation recoil momentum from the  $^{nat}\text{Ca}(p,x)^{35}\text{Ar}$  reaction may be at the origin of the release. If the protons and neutrons are not evaporated in an isotropic way, but in a preferred direction then a recoil momentum could be imposed on the produced isotope.

In order to know the average recoil energy of each  $^{35}\text{Ar}$ , FLUKA was also used<sup>4</sup>. The obtained value was  $9.2 \pm 1.8 \text{ keV}$ , exceeding the

<sup>2</sup> FLUKA simulation parameters for benchmarking: FLUKA was coupled with DPMJET-III [31] and “Hadrontherapy” was used as the default setting for more precise results.

<sup>3</sup> CaO nanopowder thermal conductivity was assumed to be  $0.03 \text{ W m}^{-1} \text{ K}^{-1}$  ( $\sim 0.2\%$  of the thermal conductivity of the solid CaO [32,33]). A cylindrical geometry for thermal conduction was used [34] with the target dimensions (2 cm diameter, 20 cm length) and all the power was assumed to be deposited in the center of the cylinder (0.5 cm radius zone – approximation to the proton beam size). The heat dissipation by radiation was calculated using the Stefan-Boltzmann law [34] and an emissivity of 0.27 [32] was used for CaO.

<sup>4</sup> In the same FLUKA simulation as in<sup>2</sup> to obtain the  $^{35}\text{Ar}$  recoils energy, the sum of all the produced isotope (HEAVYION) recoil energies, from the total energy deposition (EDEP) was calculated. A filter (AUXSCORE) was applied in order to obtain the total deposited energy only from  $^{35}\text{Ar}$ . An average energy per  $^{35}\text{Ar}$  recoil was then calculated by dividing the obtained value by the respective in-target production (RESNUCLEI).



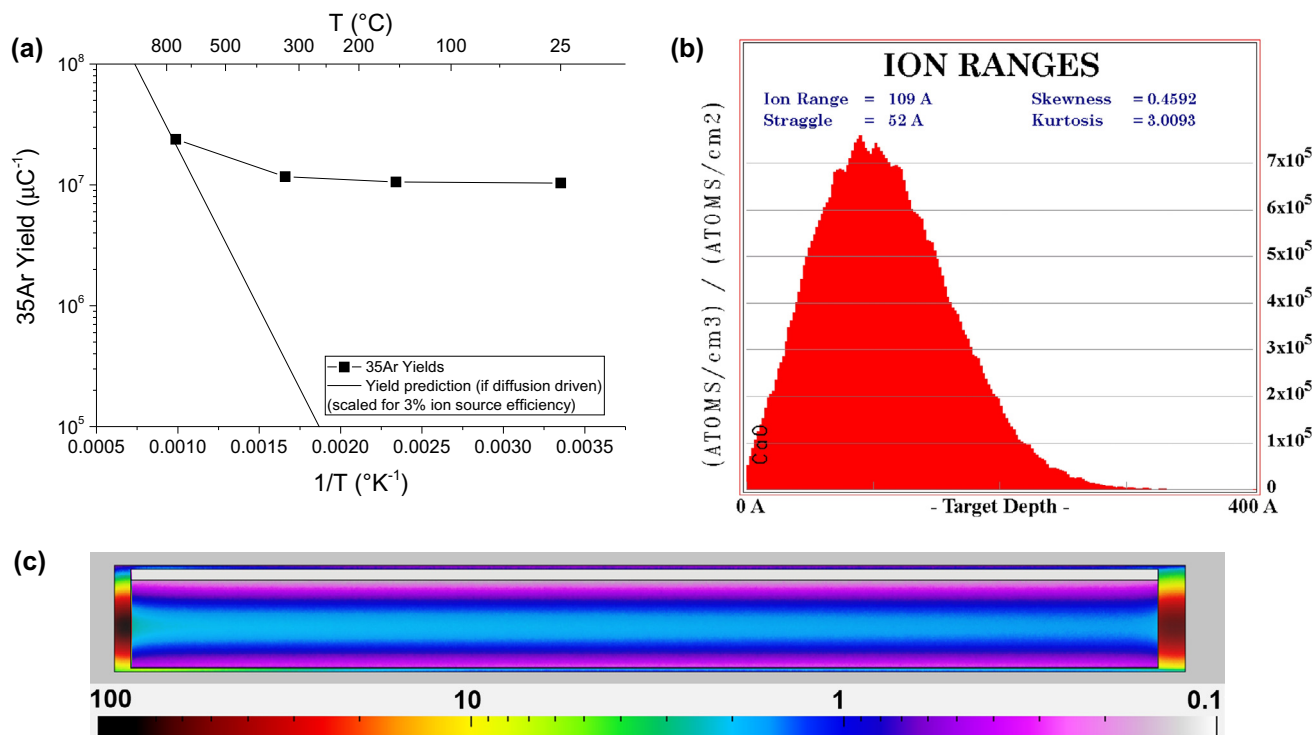


**Fig. 3.**  $^{35}\text{Ar}$  yields measured on nanometric CaO at ISOLDE while decreasing the target temperature and expected yield considering classical diffusion (see text) (a).  $^{35}\text{Ar}$  ion range when implanted (1E6 ions) in CaO with 9.21 keV – SRIM simulation (b). Total deposited energy in  $\text{W cm}^{-3}$  simulated using FLUKA when irradiating a CaO target with 2  $\mu\text{A}$ , 1.4 GeV protons (Ta container and Re support also included) (c).

binding energy of some eV. This was then used as input on SRIM (the Stopping and Range of Ions in Matter) [27,28] and the projected ion range calculated with 1E6 events, was 10.9 nm (with longitudinal and lateral straggling of 5.2 and 3.2–4.5 nm respectively), as shown on Fig. 3b. If one then considers a sphere of CaO of 40 nm diameter and uniform distribution of the produced  $^{35}\text{Ar}$ , it means that the  $^{35}\text{Ar}$  on the 10.9 nm projected range layer represents 91 vol.% of the total in the particle. The produced isotopes would then have a certain probability to escape the particle or get close to the surface (if the recoil is in the right direction). Such probability will increase with the decrease of the distance to the surface. However the isotopes that escape the particle can get implanted in a neighbour particle and the depth will depend on the kinetic energy they still have. Nonetheless, a fraction of the isotopes which are close to the surface of CaO (SSA =  $38 \text{ m}^2/\text{g}$ ), may be released, since, especially in nanomaterials, the surface tends to be highly distorted and the bonds between atoms are weaker making it easier for the non-reactive noble gas isotope to escape.

Such a release process has already been proposed but not isolated from the temperature effect [20]. The use of graphite in a  $\text{UC}_x$  target, to act as a catcher for the recoil products from the nuclear reactions was also introduced in 1978 [29]. Hydrous oxides (Zr, Ce and Th) were used as target materials to produce noble gas isotopes (Kr, Xe, and Rn), and due to decomposition (water vapour) during irradiation, they had to be operated at room temperature, but no reference was made to the possible release mechanism [30].

## 2. Conclusions

The target and ion source team at ISOLDE has gathered great expertise with the operation of various highly porous nanostructured (or composite) target materials, with apparently longer release characteristics and often higher isotope yields. However, much has still to be done in order to be able to fully understand

the release from these materials, such as modelling of the physical phenomena.

The unexpected release of Ar isotopes from a cold nanostructured CaO target points to an interesting release mechanism originating from the nuclear recoil forming an offset to the temperature dependent ion intensity at low temperatures. It is expected that this offset is especially pronounced for highly-volatile noble gases. Such release mechanism should be investigated in more depth with other cold target nanomaterials and other extracted species. However one must keep in mind that release from a cold target can only be present for volatile elements at room temperature, since the cold surfaces will lead to high effusion times.

The methods used to synthesize and engineer such nanostructures have a significant effect on material characteristics (SSA, particle size, pore size distribution, surface chemistry) which in turn will determine the release properties of a certain target, making material research still a key point in present and future ISOL facilities.

## Acknowledgements

The authors would like to acknowledge the IDS (ISOLDE Decay Station) Collaboration for the yield measurements on  $^{31}\text{Ar}$  and the ISOLDE technical team for the support.

## References

- [1] R. dos Santos Augusto, L. Buehler, Z. Lawson, S. Marzari, M. Stachura, T. Stora, CERN MEDICIS collaboration, CERN-MEDICIS (medical isotopes collected from ISOLDE): a new facility, Appl. Sci. 4 (2014) 265–281, <http://dx.doi.org/10.3390/app4020265>.
- [2] ISOLDE Newsletter Spring 2015, 31, [http://isolde.web.cern.ch/sites/isolde.web.cern.ch/files/April\\_2015\\_0.pdf](http://isolde.web.cern.ch/sites/isolde.web.cern.ch/files/April_2015_0.pdf), 2015.
- [3] T.M. Mendonca, R. Hodak, V. Ghetta, M. Allibert, D. Heuer, E. Noah, S. Cimmino, M. Delonca, A. Gottberg, M. Kronberger, J.P. Ramos, C. Seiffert, T. Stora, Production and release of ISOL beams from molten fluoride salt targets, Nucl. Instr. Meth. B 329 (2014) 1–5, <http://dx.doi.org/10.1016/j.nimb.2014.03.003>.

- [4] T.M. Mendonça, High power molten targets for radioactive ion beam production: from particle physics to medical applications, in: C. Petit-Jean-Genaz, G. Arduini, P. Michel, V.R.W. Schaa (Eds.), Proc. 5th Int. Part. Accel. Conf., JACoW, Dresden, 2014, pp. 2142–2145. <https://cds.cern.ch/record/1748357/>.
- [5] J.P. Ramos et al., in preparation.
- [6] J. Guillot et al., LaC<sub>2</sub>-C nanocomposite targets for the production of neutron-deficient spallation products at CERN-ISOLDE, in preparation.
- [7] A. Gottberg et al., Development and Online Tests of a Nano-Structured Uranium Carbide – MWCNT Composite for the Production of Rare Isotope Beams at ISOLDE-CERN, in preparation.
- [8] C. Seiffert, Production of Radioactive Molecular Beams for CERN-ISOLDE (PhD Thesis), Technische Universität Darmstadt, 2015. CERN-THESIS-2014-332, <https://cds.cern.ch/record/2064456>.
- [9] C. Seiffert et al., Development of radioactive boron beams for CERN-ISOLDE, in preparation.
- [10] J.P. Ramos, A. Gottberg, T.M. Mendonça, C. Seiffert, A.M.R. Senos, H.O.U. Fynbo, O. Tengblad, J.A. Briz, M.V. Lund, G.T. Koldste, M. Carmona-Gallardo, V. Pesudo, T. Stora, Intense 31–35Ar beams produced with a nanostructured CaO target at ISOLDE, Nucl. Instr. Meth. B 320 (2014) 83–88, <http://dx.doi.org/10.1016/j.nimb.2013.12.009>.
- [11] S. Fernandes, R. Bruetsch, R. Catherall, F. Groeschel, I. Guenther-Leopold, J. Lettry, E. Manfrin, S. Marzari, E. Noah, S. Sgobba, T. Stora, L. Zanini, Microstructure evolution of nanostructured and submicrometric porous refractory ceramics induced by a continuous high-energy proton beam, J. Nucl. Mater. 416 (2011) 99–110, <http://dx.doi.org/10.1016/j.jnucmat.2011.02.048>.
- [12] L.C. Carraz, I.R. Haldorsen, H.L. Ravn, M. Skarestad, L. Westgaard, Fast release of nuclear reaction products from refractory matrices, Nucl. Instr. Meth. 148 (1978) 217–230, [http://dx.doi.org/10.1016/0029-554X\(70\)90171-0](http://dx.doi.org/10.1016/0029-554X(70)90171-0).
- [13] J.P. Ramos, C.M. Fernandes, T. Stora, A.M.R. Senos, Sintering kinetics of nanometric calcium oxide in vacuum atmosphere, Ceram. Int. 41 (2015) 8093–8099, <http://dx.doi.org/10.1016/j.ceramint.2015.03.007>.
- [14] J.P. Ramos, Effect of Calcium Oxide Microstructure on the Diffusion of Isotopes (Master Thesis), University of Aveiro, 2012. CERN-THESIS-2012-008, <http://cdsweb.cern.ch/record/1425438/>.
- [15] J. Lettry, R. Catherall, P.V. Drumm, P. Van Duppen, A.H.M. Evensen, G.J. Focker, A. Jokinen, O.C. Jonsson, E. Kugler, H. Ravn, ISOLDE Collaboration, Pulse shape of the ISOLDE radioactive ion beams, Nucl. Instr. Meth. B 126 (1997) 130–134, [http://dx.doi.org/10.1016/S0168-583X\(96\)01025-7](http://dx.doi.org/10.1016/S0168-583X(96)01025-7).
- [16] A. Gottberg, Target Materials for Exotic ISOL Beams, Nucl. Instr. Meth. B, this issue, <http://dx.doi.org/10.1016/j.nimb.2016.01.020>.
- [17] L. Penescu, R. Catherall, J. Lettry, T. Stora, Development of high efficiency versatile arc discharge ion source at CERN-ISOLDE, Rev. Sci. Instrum. 81 (2010) 02A906, <http://dx.doi.org/10.1063/1.3271245>.
- [18] R. Kirchner, On the release and ionization efficiency of catcher-ion-source systems in isotope separation on-line, Nucl. Instr. Meth. B 70 (1992) 186–199, [http://dx.doi.org/10.1016/0168-583X\(92\)95930-P](http://dx.doi.org/10.1016/0168-583X(92)95930-P).
- [19] E. Bouquerel, Atomic Beam Merging and Suppression of Alkali Contaminants in Multi Body High Power Targets: Design and Test of Target and Ion Source Prototypes at ISOLDE (PhD Thesis), Université Paris XI, 2009. CERN-THESIS-2010-057, <http://cds.cern.ch/record/1259908>.
- [20] T. Stora, E. Noah, R. Hodak, T.Y. Hirsh, M. Hass, V. Kumar, K. Singh, S. Vaintraub, P. Delahaye, H. Franberg-Delahaye, M.-G. Saint-Laurent, G. Lhersonneau, A high intensity 6He beam for the  $\beta$ -beam neutrino oscillation facility, Europhys. Lett. 98 (2012) 32001, <http://dx.doi.org/10.1209/0295-5075/98/32001>.
- [21] G. Battistoni, F. Cerutti, A. Fassò, A. Ferrari, S. Muraro, J. Ranft, S. Ranft, S. Roesler, P.R. Sala, The FLUKA code: description and benchmarking, in: AIP Conf. Proc., AIP, 2007, pp. 31–49, <http://dx.doi.org/10.1063/1.2720455>.
- [22] A. Ferrari, P.R. Sala, A. Fassò, J. Ranft, FLUKA: A Multi-Particle Transport Code Fluka, 2005, <http://dx.doi.org/10.5170/CERN-2005-010>.
- [23] M. Domsbky, P. Bricault, P. Schmor, M. Lane, ISAC target operation with high proton currents, Nucl. Instr. Meth. B 204 (2003) 191–196, [http://dx.doi.org/10.1016/S0168-583X\(02\)01902-X](http://dx.doi.org/10.1016/S0168-583X(02)01902-X).
- [24] M. Domsbky, P. Bricault, V. Hanemaayer, Increasing beam currents at the TRIUMF-ISAC Facility: techniques and experiences, Nucl. Phys. A 746 (2004) 32–39, <http://dx.doi.org/10.1016/j.nuclphysa.2004.09.060>.
- [25] G.J. Dienes, A.C. Damask, Radiation enhanced diffusion in solids, J. Appl. Phys. 29 (1958) 1713, <http://dx.doi.org/10.1063/1.1723032>.
- [26] D.R. Lide, Handbook of Chemistry and Physics, 84th ed., CRC Press, New York, 2003.
- [27] J.F. Ziegler, M.D. Ziegler, J.P. Biersack, SRIM – the stopping and range of ions in matter, Nucl. Instr. Meth. B 268 (2010) 1818–1823, <http://dx.doi.org/10.1016/j.nimb.2010.02.091>.
- [28] J.F. Ziegler, The stopping and range of ions in matter – Simulation software, 2013, <http://www.srim.org/>.
- [29] S. Borg, I. Bergström, G.B. Holm, B. Rydberg, L.-E. De Geer, G. Rudstam, B. Grapengiesser, E. Lund, L. Westgaard, On-line separation of isotopes at a reactor in studsvik (OSIRIS), Nucl. Instr. Meth. 91 (1971) 109–116, [http://dx.doi.org/10.1016/0029-554X\(71\)90646-X](http://dx.doi.org/10.1016/0029-554X(71)90646-X).
- [30] H.L. Ravn, S. Sundell, L. Westgaard, Target techniques for the isolde on-line isotope separator, Nucl. Instr. Meth. 123 (1975) 131–144, [http://dx.doi.org/10.1016/0029-554X\(75\)90089-0](http://dx.doi.org/10.1016/0029-554X(75)90089-0).
- [31] S. Roesler, R. Engel, J. Ranft, The Monte Carlo Event Generator DPMJET-III, Adv. Monte Carlo Radiat. Physics, Part. Transp. Simul. Appl., Springer Berlin Heidelberg, Berlin, Heidelberg, 2001, pp. 1033–1038, [http://dx.doi.org/10.1007/978-3-642-18211-2\\_166](http://dx.doi.org/10.1007/978-3-642-18211-2_166).
- [32] G. Samsonov, The Oxide Handbook, Springer US, New York, 1973.
- [33] L. Huang, M.S. El-Genk, Thermal conductivity measurements of alumina powders and molded Min-K in vacuum, Energ. Convers. Manage. 42 (2001) 599–612, [http://dx.doi.org/10.1016/S0196-8904\(00\)00085-6](http://dx.doi.org/10.1016/S0196-8904(00)00085-6).
- [34] T.L. Bergman, A.S. Lavine, F.P. Incropera, D.P. DeWitt, Fundamentals of Heat and Mass Transfer, seventh ed., John Wiley & Sons, Inc., New York, 2011.